Experimental Demonstration of Energy-Chirp Control in Relativistic Electron Bunches Using a Corrugated Pipe

P. Emma,* and M. Venturini
Lawrence Berkeley National Laboratory, Berkeley, California 94720, USA

K. L. F. Bane, and G. Stupakov
SLAC National Accelerator Laboratory, Menlo Park, California 94025, USA

H.-S. Kang, M. S. Chae, J. Hong, C.-K. Min, H. Yang, T. Ha, W. W. Lee, C. D. Park, S. J. Park, and I. S. Ko
Pohang Accelerator Laboratory, Pohang 790-784, Republic of Korea
(Received 30 September 2013; published 23 January 2014)

The first experimental study is presented of a corrugated wall device that uses wakefields to remove a linear energy correlation in a relativistic electron beam (a "dechirper"). Time-resolved measurements of both longitudinal and transverse wakefields of the device are presented and compared with simulations. This study demonstrates the feasibility to employ a dechirper for precise control of the beam phase space in the next generation of free-electron-lasers.

DOI: 10.1103/PhysRevLett.112.034801 PACS numbers: 41.60.Cr

Modern x-ray free-electron-lasers (FELs) can provide high-power, ultrashort radiation for a wide range of applications in biology, chemistry, physics, and material sciences. The linear accelerator driving the FEL requires precise control of the electron bunch phase space, including compression to high peak currents and providing a constant energy along the bunch's length. The magnetic compression employed in such FELs typically leaves an undesired time-energy correlation in the bunch (an energy chirp), which can broaden the FEL bandwidth. While the chirp can be removed in a following linac section by a combination of rf phasing and the wakefields of the accelerating structures (e.g., [1]), this solution can be costly or impractical in next-generation FELs [2–4].

For such cases, it was recently proposed to insert a relatively short, dedicated structure in the accelerator driver, one that can intentionally generate strong longitudinal wakefields that "dechirp" the beam. Such a passive wakefield device—a "dechirper"—can result in considerable cost savings and/or improved FEL performance. Structures that have been proposed for use as dechirpers are a dielectric-lined waveguide [5,6], a resistive pipe of small radius [7], or a metallic structure with corrugated walls [8]. Note that in addition to the longitudinal wake that can correct a chirp, all these devices can induce strong transverse wakes which, if not properly controlled, will increase the beam projected emittance and lead to deterioration of FEL performance. Measurement of these wakefields is highly desirable prior to inclusion of a dechirper into a practical FEL design.

It is the purpose of this Letter to report the first experimental study of a corrugated-wall dechirper [8], in particular, one with a rectangular cross section and adjustable jaws. The experiment was conducted at the PAL-ITF, an electron test accelerator at the Pohang Accelerator Laboratory in Pohang, Republic of Korea, designed to test and develop the injector technology for the PAL-XFEL [2]. A rectangular geometry will be used for the PAL-XFEL, since it provides operational flexibility and can be effective for variable bunch charge and length.

The geometry of the dechirper is shown in Fig. 1. The corrugations are characterized by period p, height h, and aspect ratio h/t; the vacuum chamber has a gap $g = 2a$ and width w. In the experiment, an aluminum structure of 1 m length was used, with parameters $p = 0.5$ mm, $h = 0.6$ mm, $t = 0.3$ mm, and $w = 50$ mm. The gap g was varied from $g = 5$ mm to $g = 28$ mm.

Two methods were employed for obtaining the wakefields of the corrugated structure. Assuming that the corrugation dimensions are much smaller than the gap g, and that the frequencies of interest ω are much smaller than c/p (with c the speed of light), an analytical theory of wakefields generated by a point charge in such devices was developed in [9,10]. In a second, more accurate analysis from [9], Maxwell's equations are solved in a corrugated structure using a field-matching approach.

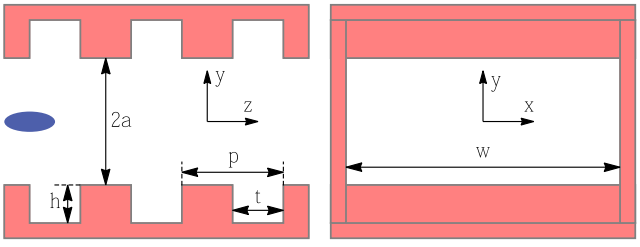

FIG. 1 (color online). Geometry of the vacuum chamber with corrugated walls. A rectangular coordinate system is centered on the symmetry axis of the chamber. The blue ellipse represents an electron beam propagating along the z axis.

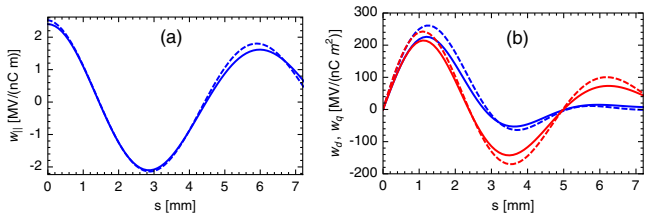

FIG. 2 (color online). Wake of the experimental structure with $g = 6$ mm, as calculated with the analytical model (dashed lines) and by using the mode-matching numerical method (solid lines): (a) the longitudinal, w_z, (b) the dipole, w_d, (blue) and quadrupole, w_q, (red) wake functions.

The wake is calculated neglecting a transient effect at the entrance of the structure—an approximation valid for our experiment. In the limit of a wide chamber, $w \gg g$, assuming an on-axis beam ($x = y = 0$), the longitudinal wake $w_z(s)$ has a cosinelike behavior, with maximal value $Z_0 c\pi/(16a^2)$, where $Z_0 = 377\ \Omega$, located at the origin, and first zero at $s = 0.22\lambda$, with $\lambda = 2\pi\sqrt{aht/p}$. The longitudinal wake for the experimental structure with $g = 6$ mm ($\lambda = 6.5$ mm), as calculated following the analytical (numerical) method, is shown in Fig. 2(a) as a dashed (solid) line.

A beam offset from the z axis experiences a transverse wake in addition to the longitudinal one. Near the axis and assuming $w \gg g$, the transverse wake between two particles can be written in terms of dipole and quad wake functions $w_d(s)$, $w_q(s)$ as

$$w_y(s) = w_d(s)y_l + w_q(s)y_t, \qquad w_x(s) = w_q(s)(x_l - x_t) \quad (1)$$

with y_l, x_l, the offsets of the leading particle and y_t, x_t, the offsets of the trailing one. Note that if all particles in the beam have the same offset, then in y the dipole and quadrupole terms add giving $w_y(s) = [w_d(s) + w_q(s)]y$, with $y \equiv y_t = y_l$, and $w_x(s) = 0$.

In a derivation using the dielectric-magnetic layer model, which we do not present here, we calculated also the transverse wake functions $w_d(s)$ and $w_q(s)$; both functions depend on the gap as $\propto a^{-4}$. The plots of the dipole and quadrupole wakes for the experimental structure (gap $g = 6$ mm) calculated using the dielectric-magnetic model are shown in Fig. 2(b) by dashed lines. The solid curves show the results of the field-matching analysis. Note that it is these functions that will be convoluted with the bunch longitudinal distribution and used in computer simulations for comparison with the experimental results.

The PAL-ITF beam line layout is shown in Fig. 3 and consists of an S-band (2856 MHz) rf photocathode gun (beam charge $Q = 200$ pC), two 3-m long S-band accelerating structures (beam energy, E_0, of 70 MeV), a 1-m long S-band vertical rf deflector (0.5 MV) [11], a horizontal bend (30 deg) with electron spectrometer line, three quadrupole focusing magnets (all switched off here), and various beam screens. For this experiment, a 1-m long corrugated

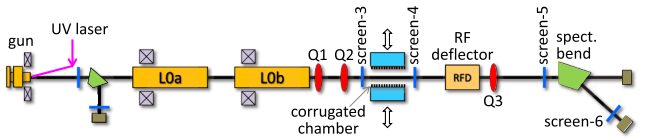

FIG. 3 (color online). Layout of the PAL-ITF wakefield experiment.

rectangular vacuum chamber was added following the second accelerating structure (L0b). The chamber support includes two separate motors allowing independent vertical positioning of each corrugated jaw, providing remote control of the full vertical gap ($g = 2a$) and its vertical offset.

All beam data are taken from one of four well-placed intercepting YAG:Ce (Cerium-doped Yttrium aluminum garnet) beam screens providing electron beam position and rms beam size (x and y) using a 5-Mpx CCD camera with 9 μm/pixel resolution. Screens 3 and 4 (Fig. 3) provide a measure of the beam size in the corrugated chamber, while screens 5 and 6 allow time-resolved measurements of both the longitudinal and transverse wake effects. We start by describing the longitudinal measurements.

In order to measure the wakefield-induced energy chirp, screen 6 is used to reconstruct the longitudinal phase space by switching on the vertical rf deflector. In this way the screen's y axis becomes the time coordinate along the bunch length, while the x axis, due to the bend, becomes the energy coordinate. The y axis is calibrated in rf degrees or ps (0.97 ps = 1 deg) by varying the rf deflector's phase ± 5 deg around its zero-crossing while recording the change of the beam's y position, converting vertical millimeters on the screen to degrees of rf phase. Similarly, its x axis is calibrated by varying the bend's magnetic field $\pm 1\%$ around its nominal 30-deg angle while recording the beam's x position, converting horizontal millimeters on the screen to percent of relative bend field (or relative energy, $\Delta E/E_0$).

For comparing the measured strength of the wake effects with simulations, the beam longitudinal profile is an important function. The bunch shape on screen 6—the longitudinal phase space with the energy coordinate integrated out—is shown in Fig. 4; the measured result is in

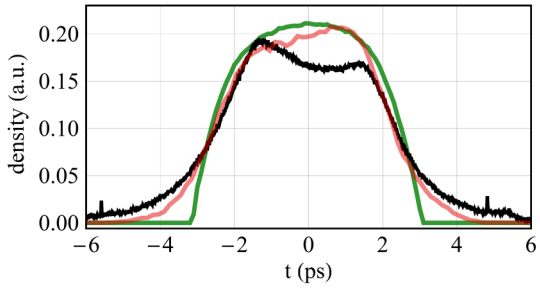

FIG. 4 (color online). Measured (black) and simulated (red) temporal profiles as seen on screen 6, compared to the fully resolved simulated profile at the dechirper (green).

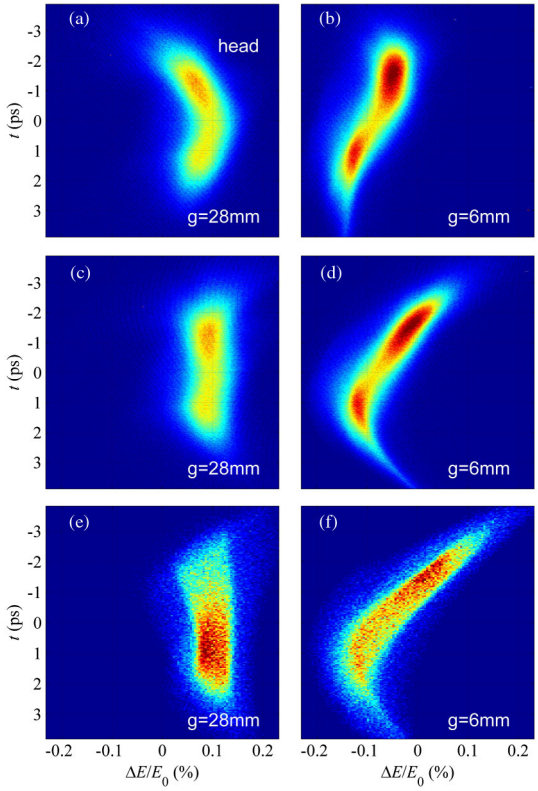

FIG. 5 (color online). Screen-6 images (*top-row*: measured, *middle-row*: measured and corrected, *bottom-row*: simulated and corrected) taken with rf deflector switched on and a net accelerating rf phase near crest. The left column of images has the gap open, and the right has the gap closed. The simulation uses 150 pC, rather than 200 pC, for better agreement with measurements.

black and the simulated result in red, for comparison. The length of both distributions is 4.8 ps FWHM. The green curve in the plot displays the simulated bunch profile at the location of the dechirper, which one can see is similar to a parabolic distribution. Tails (not present in the *green* curve) arise from a limited temporal measurement resolution on the screen. Two codes were used in the simulations: ASTRA [12] for beam propagation from the gun through L0b, and ELEGANT [13] for downstream of L0b. The simulations start at the cathode and include the measured drive laser pulse length and the gun rf phase and gradient based on the setup of the machine at the time of the experiment.

Figure 5 shows examples of measured (top 4 images), and simulated (bottom 2 images) beam. The left column is taken with the gap open ($g = 28$ mm), while the right column is with the gap closed ($g = 6$ mm). The top row of the plots shows the raw measured screen data. The next two rows include a correction for the quadratic energy chirp, dominated by the rf curvature, in order to better see the wake-induced chirp. Figure 5(d) can be directly interpreted as the energy chirp caused by the corrugated vacuum-chamber insertion and should be compared to the

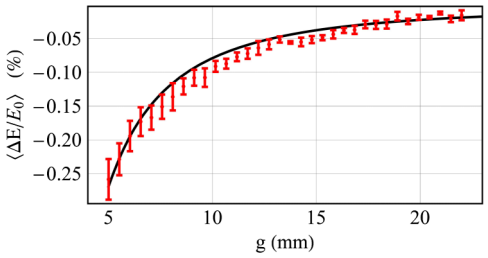

FIG. 6 (color online). Average relative energy loss over the bunch vs gap of the corrugated chamber. Error bars represent the rms variation (divided by $\sqrt{N-1}$) over $N = 4$ separate measurements spanning two days. The solid curve is a simulation using 150 pC and the measured FWHM bunch length of 4.8 ps.

simulation in Fig. 5(f). We find that the recorded beam images are best reproduced by macroparticle simulations with $Q \simeq 150$ pC bunch charge rather than the measured but somewhat uncertain 200 pC. Note these time-resolved images are single beam shots and show significant variability, whereas the well-averaged energy-loss measurements below are a better indicator of the scale.

Energy-loss measurements are made by recording the beam-centroid horizontal position on screen 6 as the dechirper gap is varied from 5 to 28 mm. We again find the simulations require a bunch charge of 150 pC to fit the measurements better (see Fig. 6). Note the rf deflector is switched off for these centroid measurements.

In addition to longitudinal wakes, the beam line arrangement is well suited for measurement of the transverse

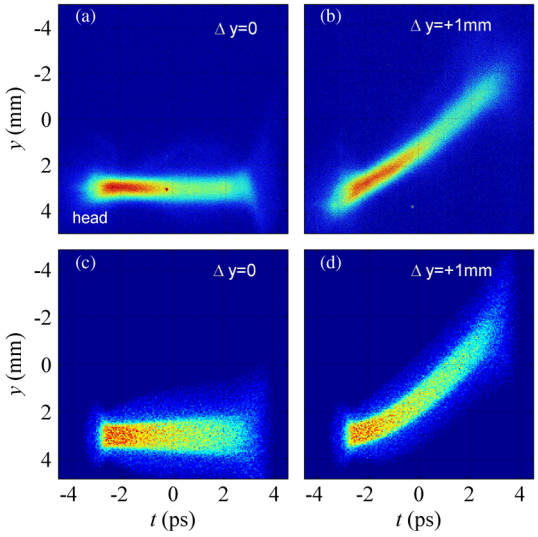

FIG. 7 (color online). Screen 6 images (*top-row*: measured, *bottom-row*: simulated, $Q = 150$ pC), with $g = 6$ mm, rf deflector switched off and L0a phase adjusted 10 degrees off crest, showing no dipole kick when gap is centered on the beam (*left*), but a strong tail kick with gap off axis by 1 mm (*right*). The bunch head is at left in each image.

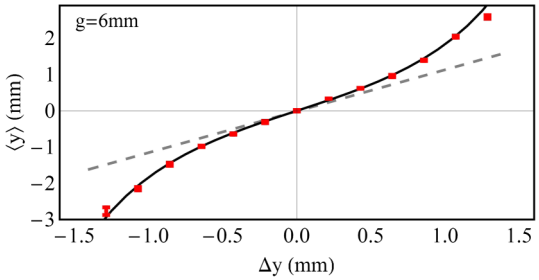

FIG. 8 (color online). Measured (red) average vertical beam position on screen 5 vs vertical offset of the gap ($g = 6$ mm) against ELEGANT simulations (dashed line) based on a linear approximation of the transverse wake and a calculation (solid line) including the wake nonlinearities for a parabolic bunch ($Q = 150$ pC in both simulation cases).

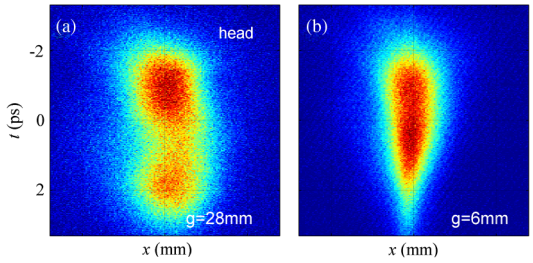

FIG. 9 (color online). Screen 5 measured images with the rf deflector switched on, showing no quadrupole wake when the gap is open (*left*), but a strong time-dependent horizontal focusing with the gap closed to $g = 6$ mm (*right*). The bunch head is at the top.

wakefields. With the rf deflector switched off and L0a (Fig. 3) rf phase adjusted to about 10 degrees off its accelerating crest, a strong linear energy chirp can be induced, converting the x axis of screen 6 to time. This configuration provides a time-resolved measure of the vertical kick of a vertically off-axis beam in the gap. Figure 7 reports measured (top row) and 150-pC simulated (bottom row) beam images on screen 6. The 6-mm gap is vertically centered on the beam in the left two images, but the gap is 1 mm offset in the right two images. The x axes are calibrated in ps by varying the L0a rf phase ± 2 deg around its 10-deg setting while recording the beam's x position. Horizontal millimeters on the screen are then converted to degrees of rf phase (or ps). Note that the kick at the tail of the bunch is quite significant (the bunch head is at left). The vertical center of the gap was confirmed by scraping the beam slightly at each extreme of vertical position.

A detailed investigation of the average vertical kick induced by the transverse wake as a function of the vertical offset of the dechirper gap is best carried out by monitoring the beam on screen 5 (with the rf deflector turned off). The data collected with $g = 6$ mm gap setting, Fig. 8, show a strong nonlinear behavior, which is well reproduced by the transverse-wake model applied to a parabolic bunch with 4.8-ps FWHM length and $Q = 150$ pC, solid line. The dashed line is from ELEGANT simulations, where the transverse wake is modeled in linear approximation.

Finally, turning on the rf deflector enables screen 5 to record time-resolved measurements, including horizontal time-dependent focusing along the bunch produced by quadrupole wakes (see Fig. 9). The observed beam features are reasonably well reproduced by simulations (not shown) with 150 pC bunch charge.

The quadrupole wake results in projected-emittance growth. For the beam on axis, we measured the emittance for several values of the gap. We find that when $g = 6$ mm, the projected vertical emittance grows by a factor of four compared to the $g = 28$ mm case, in good agreement with analytical calculations. While of serious concern, we should notice that this growth critically depends on the machine and beam parameters. For example, analytical estimates and simulations show that in the PAL-XFEL, with a much shorter bunch length and higher beam energy, employing a similar rectangular-aperture dechirper to remove the energy chirp would cause only 10% emittance growth.

In conclusion, these time-resolved measurements confirm both the linearity and the approximate scale of the wake-induced chirp of the corrugated chamber, as predicted by the wakefield model. We obtain reasonably good agreement between measurement and model in both the longitudinal and transverse planes if we regard the bunch charge as a fitting parameter and choose $Q = 150$ pC, (i.e., a value 25% smaller than the measured but uncertain value of 200 pC). Our results give one confidence in the practicality of including a corrugated-wall dechirper in the design of next-generation FELs.

Work supported in part by the U.S. Department of Energy under Contracts No. DE-AC02-76SF00515 and No. DE-AC02-05CH11231.

*Corresponding author.Emma@SLAC.Stanford.edu

[1] P. Emma *et al.*, Nat. Photonics **4**, 641 (2010).
[2] J.-H. Han, H.-S. Kang, and I. S. Ko, in Proceedings of 2012 International Particle Accelerator Conference, New Orleans, p. 1735, http://www.jacow.org/.
[3] J. Corlett *et al.* in Proceedings of the 2013 FEL Conference, New York, 2013 (to be published).
[4] SwissFEL Conceptual Design Report, Tech. Report No. 10-04, 2012.
[5] S. Antipov, C. Jing, M. Fedurin, W. Gai, A. Kanareykin, K. Kusche, P. Schoessow, V. Yakimenko, and A. Zholents, Phys. Rev. Lett. **108**, 144801 (2012).
[6] S. Antipov, S. Baturin, C. Jing, M. Fedurin, A. Kanareykin, C. Swinson, P. Schoessow, W. Gai, and A. Zholents, arXiv:1308.5646.

[7] H.-S. Kang, J.-H. Han, T. H. Kang, and I. S. Ko, in Proceedings of the FEL Conference, Nara, Japan, 2012, edited by T. Tanaka (JACoW, 2013), p. 309.
[8] K. L. F. Bane and G. Stupakov, Nucl. Instrum. Methods Phys. Res., Sect. A **690**, 106 (2012).
[9] K. L. F. Bane and G. V. Stupakov, Phys. Rev. ST Accel. Beams **6**, 024401 (2003).
[10] G. Stupakov and K. L. F. Bane, Phys. Rev. ST Accel. Beams **15**, 124401 (2012).
[11] R. Akre, L. Bentson, P. Emma, and P. Krejcik, in Proceedings of the 2001 Particle Accelerator Conference, Chicago, 2011, edited by P. Lucas (IEEE, New York, 2001), p. 2353.
[12] K. Flöttmann, ASTRA: A Space Charge Tracking Algorithm, DESY Tech. Rep., http://www.desy.de/~mpyflo, 2011.
[13] M. Borland, Tech. Report No. LS-287 Advanced Photon Source, 2000.